Research Article | Vol. 28, No. 6 / 16 March 2020 / Optics Express 8724
Optics EXPRESS

27 W 2.1 µm OPCPA system for coherent soft X-ray generation operating at 10 kHz

TIANLI FENG,[1,2,4] ANKE HEILMANN,[1,5] MARTIN BOCK,[1] LUTZ EHRENTRAUT,[1] TOBIAS WITTING,[1] HAOHAI YU,[3] HOLGER STIEL,[1] STEFAN EISEBITT,[1] AND MATTHIAS SCHNÜRER[1]

[1]*Max-Born-Institut, Max Born Straße 2a, 12489 Berlin, Germany*
[2]*School of Information Science and Engineering, Shandong University, Qingdao 266237, China*
[3]*State Key Laboratory of Crystal Materials, Institute of Crystal Materials, Shandong University, Jinan 250100, China*
[4]*feng@mbi-berlin.de*
[5]*heilmann@mbi-berlin.de*

Abstract: We developed a high power optical parametric chirped-pulse amplification (OPCPA) system at 2.1 µm harnessing a 500 W Yb:YAG thin disk laser as the only pump and signal generation source. The OPCPA system operates at 10 kHz with a single pulse energy of up to 2.7 mJ and pulse duration of 30 fs. The maximum average output power of 27 W sets a new record for an OPCPA system in the 2 µm wavelength region. The soft X-ray continuum generated through high harmonic generation with this driver laser can extend to around 0.55 keV, thus covering the entire water window (284 eV - 543 eV). With a repetition rate still enabling pump-probe experiments on solid samples, the system can be used for many applications.

1. Introduction

The use of femtosecond soft X-ray (SXR) pulses for spectroscopy is of large interest for the study of electronic dynamics with elemental and chemical sensitivity. Within this context, high-power ultrafast light sources in the near- and mid-infrared (MIR) wavelength region have attracted a lot of attention as drivers of high harmonic generation (HHG) [1–4], as they allow to reach e.g. the 1s core levels of the biologically relevant, light elements carbon, nitrogen and oxygen. Hence, they cover the so-called water window (284 eV - 543 eV), allowing for the study of biomolecules in their natural aqueous environment [5,6]. Furthermore, the associated short wavelengths in the single digit nm range lend themselves to experiments with sub-100 nm spatial resolution in reciprocal or real space [7,8].

The physics of the HHG-process in gaseous targets explains the advantageous use of MIR laser drivers when generation of SXR pulses is required [9]. However, the reported conversion efficiencies from the primary (optical) to the secondary (SXR) laser pulses are tremendously low: Under ideal conditions and with perfect phase-matching, efficiencies between 10^{-5} and 10^{-7} are predicted [3,10], while experimental values can easily be several orders of magnitude lower [11]. Hence, the photon flux required for measurements can only be realized with powerful primary laser drivers operating in the MIR wavelength region.

High-energy few-cycle MIR drivers are mainly enabled by optical parametric chirped pulse amplifiers (OPCPA) pumped with commercial high-power picosecond lasers around 1 µm [12–15]. Using such a pump laser, it is possible to obtain MIR pulses from 2 µm to 4 µm via different nonlinear crystals such as BBO [16], BiBO [17], LNO [18], PPLN [19] and KTA [20]. Operating in the 2 µm wavelength region has three main advantages: First, the radiation strength of the single atomic HHG-process increases with higher frequency [21]. However, considering the scaling of the cut-off energy with $I_L\lambda_L^2$ (I_L: laser intensity, λ_L: laser wavelength) [22], a higher wavelength is more favorable for achieving the desired HH-photon energies without excessive

#386588 https://doi.org/10.1364/OE.386588
Journal © 2020 Received 23 Dec 2019; revised 19 Feb 2020; accepted 25 Feb 2020; published 11 Mar 2020

Optics EXPRESS

ionization of the target. Therefore 2 µm light pulses are a good compromise to realize HHG in the water window [23]. Second, considering that the gain of the signal pulse is inversely proportional to its wavelength, 2 µm pulses are much easier to amplify to a high energy level than longer wavelength signals. Third, both the seed and idler pulses cover a similar spectral range in a degenerate OPCPA system operating in the 2 µm wavelength region. This results in a small group velocity difference between the signal and idler pulses, which is favorable for maintaining the broad spectral bandwidth of the signal pulse needed for generating few-cycle pulses.

However, previous studies have shown that high average output power is very difficult to achieve from a 2 µm OPCPA system. This can be seen in Fig. 1 which summarizes the 2 µm OPCPA systems reported in the literature [16–18,24,25]. The maximum average output powers are limited to about 10 W, and only recently this value was surpassed with a 100 kHz repetition rate OPCPA system [19].

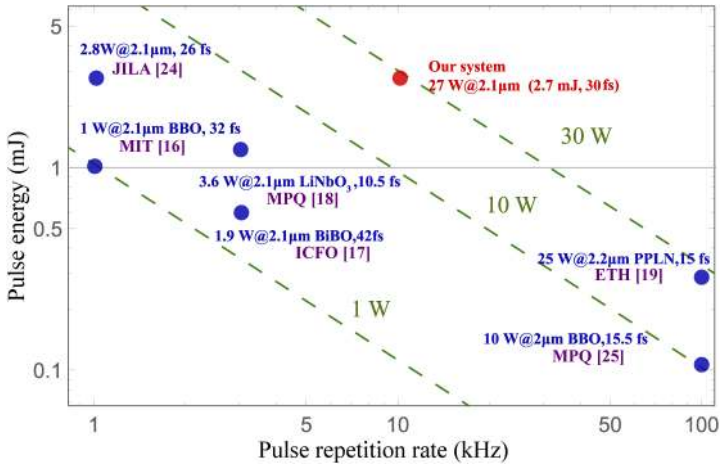

Fig. 1. OPCPA systems reported in the literature operating around 2 µm wavelength. The x-axis indicates the pulse repetition rate and the y-axis indicates the single pulse energy. Our system reported in this paper is marked with red color. 1 mJ pulse energy is indicated by a gray horizontal line.

Furthermore, there are currently no 2 µm OPCPA systems with pulse repetition rates between 5 kHz and 20 kHz. However, these are of particular interest for pump-probe soft X-ray spectroscopy on solid samples, since they balance the signal-to-noise advantages of high frequency detection with the power levels tolerable on such a sample [26,27].

Enhancing the average output power to more than 10 W at the above-mentioned pulse repetition rates while realizing multi-mJ pulse energies is greatly restricted by the currently available nonlinear crystals. Typically, these nonlinear crystals include BBO, BiBO, LNO, and PPLN. Although BBO and BiBO crystals have high damage thresholds (~ 100 GW/cm^2 @ 1 ps), they are usually not suitable for high power operation in the 2 µm wavelength region due to the strong absorption (see Fig. 2). LNO and PPLN are transparent around 2 µm, which in principle can support high power output if the photorefractive effect could be properly suppressed. In Ref. [19], the photorefractive effect in PPLN crystal is mitigated by lowering down the pumping intensity, which is realized with a high-aspect ratio poled aperture crystal (2×10.9 mm^2) and a flattened pumping beam. This eventually enables a maximum average output power of 25 W. However, power upscaling needs larger apertures which are not available so far.

Compared with the above-mentioned nonlinear crystals, YCOB (short for $YCa_4O(BO_3)_3$) as a monoclinic biaxial crystal has a high damage threshold comparable with BBO or BiBO and a good transmittance which is not inferior to LNO or PPLN (see Fig. 2) [28]. The relatively

Optics EXPRESS

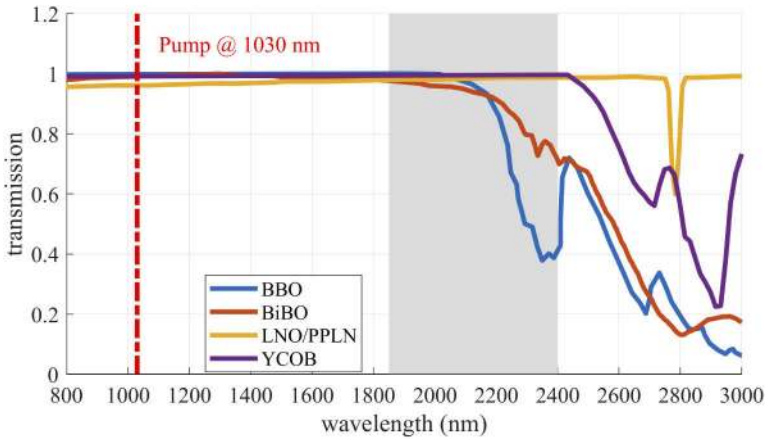

Fig. 2. The transmissions through 1 cm sample for different nonlinear crystals. The dashed red line marks the pump wavelength and the gray area marks the spectrum of the signal pulse (The curves are obtained from [30] and [31]).

low nonlinear coefficient of ~ 1 pm/V can be outweighed by the large available crystal sizes. Indeed, YCOB crystals up to 5 inch in diameter and 200 mm in length have been successfully grown by using Czochralski method at present, which can be converted to a single crystal with an aperture of several centimeters [29]. In conclusion, with a good transparency in the 2 µm wavelength region and large available sizes, YCOB crystals should be very suitable for a 2 µm OPCPA system.

In this paper, we demonstrate for the first time a high power 10 kHz 2.1 µm OPCPA where both pump and signal stem from one and the same 500 W Yb:YAG thin disk laser. Our system yields a maximum average output power of 27 W with a single pulse energy of 2.7 mJ, a pulse duration of 30 fs, and an excellent beam quality of $M^2 = 1.1$. To the best of our knowledge, this is the highest average output power which has ever been achieved from a 2 µm OPCPA system. We also demonstrate HHG with this laser system, which yields an SXR continuum covering the whole water window wavelength region (284 eV - 543 eV).

2. Layout of the 2.1 µm OPCPA system

A schematic diagram of our 2.1 µm OPCPA system is shown in Fig. 3. The pump source is a commercial Yb-doped 10 kHz thin-disk regenerative amplifier (Dira 500-10, Trumpf Scientific Lasers) with a total average output power of 500 W and a pulse duration of 2 ps (0.9 ps Fourier limit). To optically synchronize the pump pulse and the seed pulse, a part of the pump pulse (~ 0.5 mJ) is separately compressed to ~ 1 ps for pumping a commercial 2.1 µm front-end (Fastlite). The seed pulse is generated from a fraction of this 0.5 mJ pump pulse via two cascaded nonlinear processes, i.e., supercontinuum generation (SCG) and difference frequency generation (DFG), before it is amplified with two subsequent OPA stages using PPLN as nonlinear crystals. Between these two OPA stages, an acousto-optic programmable dispersive filter (AOPDF, Dazzler, Fastlite) is employed for dispersion management. The spectrum of the seed pulse extends from 1800 nm to 2600 nm with a central wavelength of 2.1 µm [32], so that the strong water absorption in air around 1.9 µm is located at the edge of the spectrum. With proper dispersion control, the seed pulse could be compressed down to 19 fs. We run the front-end at ~ 27 µJ (270 mW) by tuning the AOPDF in order to compensate the residual group delay dispersion (GDD) and third order dispersion (TOD) in the power OPCPA system (cf. Figure 3). The seed delivered from the front-end has a pulse duration of 0.5 ps with a positive GDD of 3500 fs^2.

Optics EXPRESS

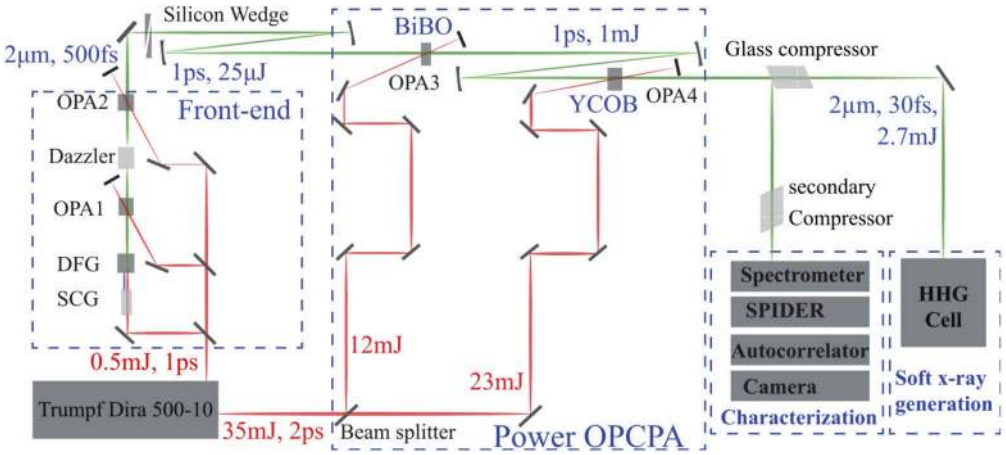

Fig. 3. Schematic diagram of the 2.1 µm OPCPA system. The 500 W Yb:YAG thin disk laser acts as both pump and signal generation source.

The largest fraction of the pump laser power (~ 35 mJ, 2 ps) is used for pumping a subsequent power OPA chain. This OPA chain is composed of two degenerated stages (OPA3 and OPA4), designed for different gain levels with a numerical code (Sisyfos, SImulation SYstem For Optical Science). To spatially separate signal and idler pulses after amplification, the signal and pump beams are crossed at a small angle (~ 2°). In order to efficiently extract the pulse energy from the pump pulse, the seed pulse is further stretched to 1 ps (GDD = + 7500 fs^2) by a pair of silicon wedges. In the stage OPA3, 12 mJ of the pump pulse is used to amplify the seed pulse from ~ 27 µJ to ~ 1 mJ with a 5 mm beam diameter ($1/e^2$) in a 2 mm thick BiBO ($\theta = 21.4°$) crystal. A further increase of pump energy in OPA3 resulted in serious distortions of the spatial beam profile. In the final OPA stage, YCOB with a thickness of 3.6 mm ($\theta = 36.7°$) is employed. The signal pulse is eventually boosted to 2.9 mJ via 23 mJ pumping with 1 cm beam diameter ($1/e^2$). Although there is still 10 mJ pumping energy per pulse unexploited, we did not further increase the pump pulse energy in the last OPA stage due to the aperture limitation of the YCOB crystal. A further increase in average output power can thus be achieved when the full pumping power is exploited via larger aperture crystals. After the final OPA stage, a 4 cm long uncoated glass block (Suprasil 300) is employed for pulse compression. The glass block is placed at an appropriate angle adjusting the propagation length in the material with a resulting GDD = -7500 fs^2. At the same time, it serves as entrance window for the subsequent vacuum system dedicated to HHG experiments. The losses due to reflections at the surfaces of the glass block reduce the total average output power to 27 W. However, these reflections provide an opportunity to perform online measurements of the spectrum and the spatial profile of the beam. By inserting a secondary glass block identical to the main one, even the duration of the compressed pulses can be evaluated.

3. Output parameters of the 2.1 µm OPCPA system

Figure 4(a) shows the output spectrum of the 2.1 µm OPCPA system, measured at the maximum output power with a spectrometer (Wavescan, APE). The spectrum extends from ~ 1.8 µm to ~ 2.5 µm with a spectral bandwidth (FWHM) of 337 nm, matching well the result of the simulation (red dashed line in Fig. 4(a)). Since the beam path of our OPCPA system is directly in air, the influence of water absorption can be clearly seen in the measured spectrum as a dip around 2 µm. The other dip at 2.2 µm is caused by the small back conversion in the OPA stages. The near field beam profile shown in Fig. 4(b) is measured via a pyroelectrical camera (Spiricon),

Optics EXPRESS

with a nearly Gaussian distributed beam intensity in the near field. The far field beam profile is measured via two-photon excitation with a Si-CCD at the focus of a 500 mm CaF_2 lens, also showing a Gaussian distributed intensity, implying there is no serious back conversion. Moreover, the M^2 parameter determination yielded a value of 1.1, indicating a nearly diffraction limited output beam. Figure 4(c) displays the comparison between measured and simulated OPA output. The observed discrepancy in the second amplifier stage at 35 mJ pump energy probably indicates a beginning mismatch of pump intensity.

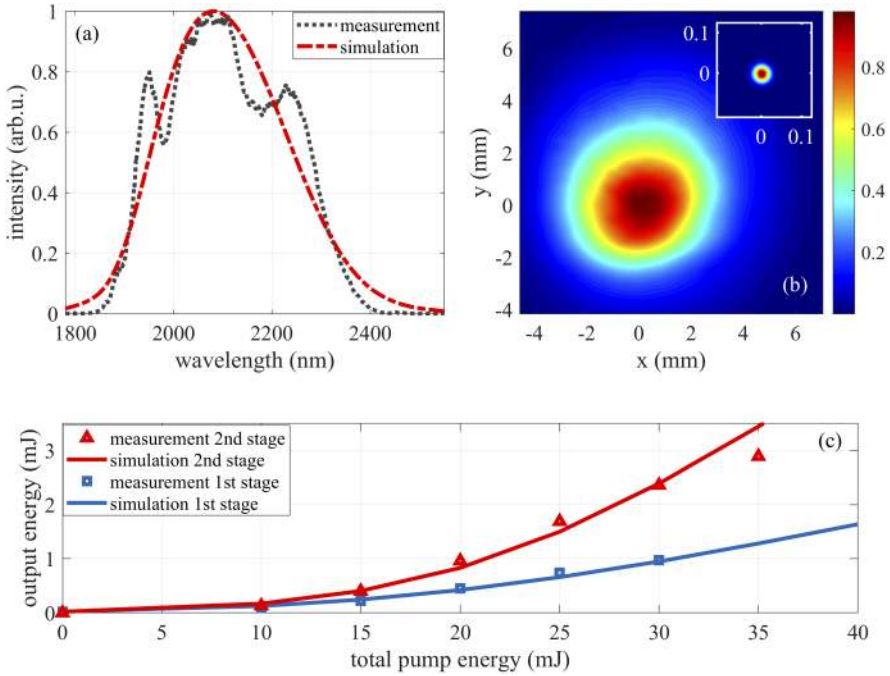

Fig. 4. The (a) output spectrum, and (b) normalized near field beam profile of the 2.1 µm OPCPA system at the maximum output power. The inset shows the focused far field beam profile obtained with a 500 mm CaF_2 lens, and has the same units as the near field figure. (c) Comparison between measured and calculated (Sisyfos software) laser system output.

The pulse energy stability of our DIRA pump laser is about 0.5 % (rms) (internal measurement of the DIRA-diagnostic). This value does not include pointing and divergence fluctuations which also contribute to the front-end signal generation stability. Hence, based on the DIRA pump laser, the front-end yields an energy stability about three to four times worse than the pump, which could not ensure a satisfactory carrier envelope phase (CEP) stability yet. An updated front-end version with a modified setup and an improved pump stability is expected to allow for the generation of CEP stable pulses as reported for a similar 3 µm system [33].

The pulse duration is measured at the maximum output power of 27 W with a homemade spatially-encoded arrangement filter-based spectral phase interferometry for direct electric field reconstruction (SEA-F-SPIDER) setup similar to the one described in [34]. Here we use an external reference (ancilla) beam for the sum-frequency mixing [35,36]. Our reference stems from parasitic second harmonic generation in the OPA stages. The reference beam has a spectrum centered around 1010 nm from which we filter out two quasi-monochromatic beams using bandpass filters (Semrock). The generated sum-frequency signal between the ancillae and short pulse beams lies in the spectral range from 655 nm to 710 nm, which coincides with the responsive range of standard silicon cameras.

Optics EXPRESS

As can be seen in Fig. 5(a), the retrieved spectrum features a largely flat phase with some small residual positive TOD. Discrepancies between the measured and the retrieved spectrum can be explained by differences in the calibration of the respective spectrometers. The retrieved temporal phase is nearly flat as well, and the pulse duration is 30 fs (cf. Figure 5(b)), corresponding to about 4 oscillation cycles at 2.1 µm. The uncompensated TOD results in a preceding and following tail pulse which only account for about 2 % of the energy of the main pulse. The pulse peak power is calculated to be ~ 90 GW.

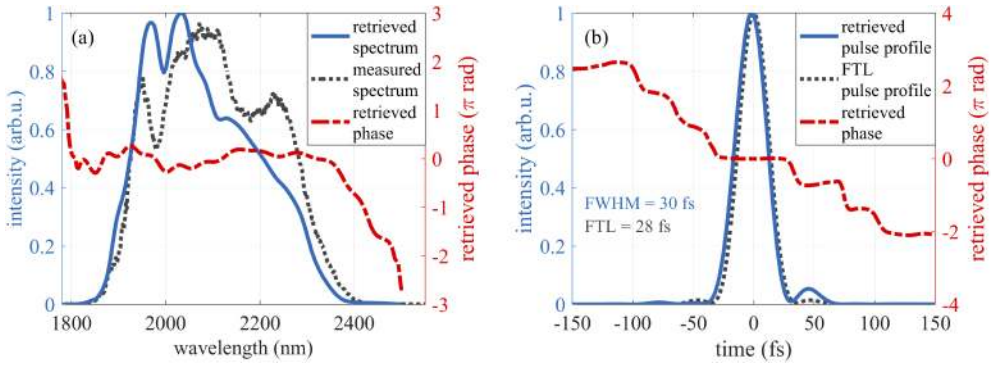

Fig. 5. Results of the SEA-F-SPIDER pulse characterization: (a) Spectral intensity and phase, (b) temporal pulse profile and phase.

4. Soft X-ray generation

A schematic of the setup used for the HHG experiments is shown in Fig. 6. The compressed 2.1 µm laser is routed into a vacuum beamline, where the 4 cm long glass compressor acts as the entrance window. A CaF_2 spherical lens is used for loosely focusing the beam in a homemade differentially pumped 6 mm long gas cell. Behind the cell, two additional vacuum chambers are used for beam separation and HHG characterization. In order to isolate the generated SXR radiation, an aperture mirror with a 4 mm central hole is employed to reflect ~ 90 % of the MIR laser. The residual MIR laser beam is reflected and to some minor extend absorbed by one or more 200 nm thick free-standing foil filter(s). The heat conductivity of the first filter needs to be sufficiently high to avoid filter damage. The spectra of the SXR radiation are measured with a transmission grating spectrograph [37], which consists of a 50 µm slit, an Si_3N_4 (10 000 lines/mm) grating and a CCD camera (Andor). The intensity of the generated SXR radiation is optimized by changing the focusing position and the target gas pressure.

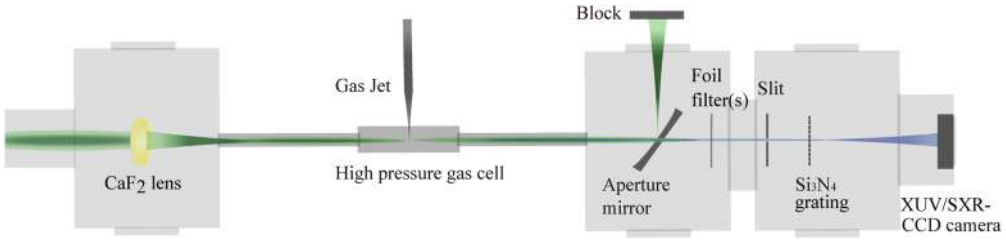

Fig. 6. The experimental setup for the HHG experiments.

The transmission grating and the CCD camera were calibrated by the German national metrology institute, Physikalisch-Technische Bundesanstalt, and the X-ray transmission curves

Optics EXPRESS

of the foil filters are taken from [38]. While these components would allow for absolute measurements of the photon flux, it is difficult to assess which fraction of the SXR beam is transmitted through the entrance slit of the spectrometer. Calculations based on the estimated beam divergence of about 1 mrad yield a ratio of 0.02, while extrapolations from measured spectra and beam profiles can lead to significantly lower results. This explains the high uncertainties in the photon numbers given below.

We first measured HHG in helium, using an f = 500 mm focal length lens and a He pressure between 1.4 bar and 2 bar depending on the focus position. At the focus, the beam is measured to be 107 µm in diameter (4σ), corresponding to a beam intensity of 9.4×10^{14} W/cm^2. Two aluminum filters are used for MIR beam removal and stray light suppression. Figure 7(a) shows the measured spectra with and without a 200 nm Ti-filter (behind the Al-filters) in the beam. The spectra are scaled relatively to each other and represent an averaging over 1.5×10^6 pulses (150 s). The K-shell absorption edges of carbon (284 eV) and nitrogen (410 eV) are visible in all measurements, originating from organic contaminants and the absorption of the Si_3N_4 grating, respectively. The photon flux from the source at the carbon K-edge of 284 eV is calculated to be $\sim (2-5) \times 10^4$ photons/s/eV and we find $\sim (0.5-1) \times 10^4$ photons/s/eV at 500 eV.

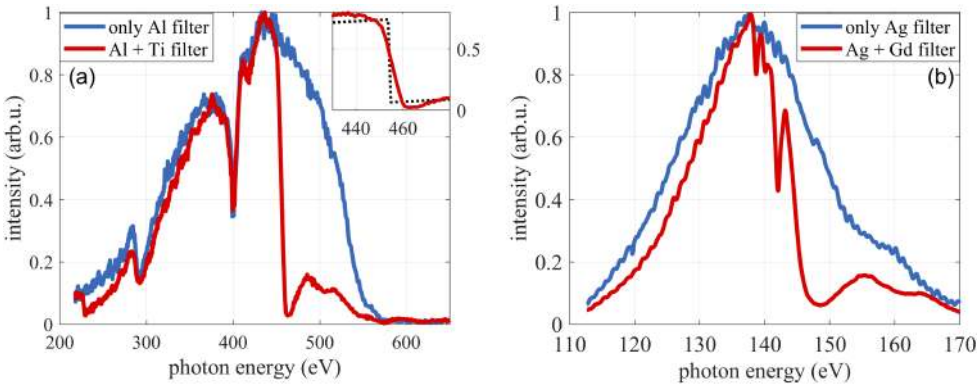

Fig. 7. (a) Normalized HHG spectra generated from 1.8 bar He with the 2.1 µm OPCPA system at 10 kHz repetition rate, where the signal is accumulated for 150 s. Inset: Zoom of the Ti-L-edge and the transmission of a 200 nm Ti foil filter [38], and (b) obtained spectrum from 240 mbar Ar, accumulated for one hour, other parameters cf. text.

These values are nominally lower than those reported for other sources in the literature [9,39], indicating that larger photons numbers could most likely be achieved with shorter driving pulses and improved gas target design. However, for similar integration times the contrast quality of our recorded absorption Ti L-edge seems to be comparable with other results (cf. inset of Fig. 7(a)) [39].

Furthermore, we also performed HHG in argon. We use a gas pressure of 240 mbar and focus the 2.1 µm beam into the gas with an f = 750 mm lens, leading to a beam diameter of 160 µm and an intensity of 4.1×10^{14} W/cm^2. A 200 nm Ag-filter was used for MIR light suppression. The resulting spectrum is shown in Fig. 7(b). Additionally, we inserted a 40 nm Gd-filter, deposited on a thin layer of diamond-like carbon and protected by 3 nm of Ta. The corresponding absorption edge is also shown in Fig. 7(b). Determined the same way as described above, the photon numbers at the source for 140 eV are $\sim (2-4) \times 10^5$ photons/s/eV.

5. Conclusion

In conclusion, we report a 10 kHz 2.1 µm OPCPA system, which delivers a single pulse energy of 2.7 mJ at a pulse duration of 30 fs. The 27 W maximum average output power surpasses

Optics EXPRESS

other OPCPA systems reported in the 2 µm wavelength region, in particular when considering repetition rates ≤ 20 kHz allowing for optical pump - SXR probe experiments on solids. Due to crystal size limitations, currently only 80 % of the available DIRA pump power is used. Scaling to higher output powers is straightforward by employing a large aperture YCOB crystal in the final OPA stage. First HHG in He and Ar driven by this 2.1 µm OPCPA system covered the expected wavelength range, including the entire water window. Furthermore, it allowed for high signal-to-noise detection of the Gd N-shell and Ti L-shell absorption edges from thin transmission filters.

Funding

European Regional Development Fund (Nanomovie); Horizon 2020 Framework Programme for Research and Innovation (654148 Laserlab-Europe); Shandong University (Qilu Young Scholars Program); Shandong Province (Taishan Young Scholars Program).

Acknowledgments

We thank G. Arisholm (Forsvarets forskningsinstitutt, Norway) for providing the Sisyfos software for OPCPA simulation.

Disclosures

The authors declare no conflicts of interest.

References

1. B. Wolter, M. G. Pullen, M. Baudisch, M. Sclafani, M. Hemmer, A. Senftleben, C. D. Schröter, J. Ullrich, R. Moshammer, and J. Biegert, "Strong-field physics with Mid-IR fields," Phys. Rev. X **5**(2), 021034 (2015).
2. X. Ren, J. Li, Y. Yin, K. Zhao, A. Chew, Y. Wang, S. Hu, Y. Cheng, E. Cunningham, Y. Wu, M. Chini, and Z. Chang, "Attosecond light sources in the water window," J. Opt. **20**(2), 023001 (2018).
3. T. Popmintchev, M.-C. Chen, D. Popmintchev, P. Arpin, S. Brown, S. Ališauskas, G. Andriukaitis, T. Balčiunas, O. D. Mücke, A. Pugzlys, A. Baltuška, B. Shim, S. E. Schrauth, A. Gaeta, C. Hernández-García, L. Plaja, A. Becker, A. Jaron-Becker, M. M. Murnane, and H. C. Kapteyn, "Bright coherent ultrahigh harmonics in the kev x-ray regime from mid-infrared femtosecond lasers," Science **336**(6086), 1287–1291 (2012).
4. A. S. Johnson, D. R. Austin, D. A. Wood, C. Brahms, A. Gregory, K. B. Holzner, S. Jarosch, E. W. Larsen, S. Parker, C. S. Strüber, P. Ye, J. W. G. Tisch, and J. P. Marangos, "High-flux soft x-ray harmonic generation from ionization-shaped few-cycle laser pulses," Sci. Adv. **4**(5), eaar3761 (2018).
5. A. R. Attar, A. Bhattacherjee, C. D. Pemmaraju, K. Schnorr, K. D. Closser, D. Prendergast, and S. R. Leone, "Femtosecond x-ray spectroscopy of an electrocyclic ring-opening reaction," Science **356**(6333), 54–59 (2017).
6. C. Kleine, M. Ekimova, G. Goldsztejn, S. Raabe, C. Strüber, J. Ludwig, S. Yarlagadda, S. Eisebitt, M. J. J. Vrakking, T. Elsaesser, E. T. J. Nibbering, and A. Rouzée, "Soft x-ray absorption spectroscopy of aqueous solutions using a table-top femtosecond soft x-ray source," J. Phys. Chem. Lett. **10**(1), 52–58 (2019).
7. B. Vodungbo, J. Gautier, G. Lambert, A. B. Sardinha, M. Lozano, S. Sebban, M. Ducousso, W. Boutu, K. Li, B. Tudu, M. Tortarolo, R. Hawaldar, R. Delaunay, V. López-Flores, J. Arabski, C. Boeglin, H. Merdji, P. Zeitoun, and J. Lüning, "Laser-induced ultrafast demagnetization in the presence of a nanoscale magnetic domain network," Nat. Commun. **3**(1), 999 (2012).
8. O. Kfir, S. Zayko, C. Nolte, M. Sivis, M. Möller, B. Hebler, S. S. P. K. Arekapudi, D. Steil, S. Schäfer, M. Albrecht, O. Cohen, S. Mathias, and C. Ropers, "Nanoscale magnetic imaging using circularly polarized high-harmonic radiation," Sci. Adv. **3**(12), eaao4641 (2017).
9. M.-C. Chen, P. Arpin, T. Popmintchev, M. Gerrity, B. Zhang, M. Seaberg, D. Popmintchev, M. M. Murnane, and H. C. Kapteyn, "Bright, coherent, ultrafast soft x-ray harmonics spanning the water window from a tabletop light source," Phys. Rev. Lett. **105**(17), 173901 (2010).
10. V.-M. Gkortsas, S. Bhardwaj, E. L. Falcão-Filho, K.-H. Hong, A. Gordon, and F. X. Kärtner, "Scaling of high harmonic generation conversion efficiency," J. Phys. B: At., Mol. Opt. Phys. **44**(4), 045601 (2011).
11. V. Cardin, B. E. Schimdt, N. Thiré, S. Beaulieu, V. Wanie, M. Negro, C. Vozzi, V. Tosa, and F. Légaré, "Self-channelled high harmonic generation of water window soft x-rays," J. Phys. B: At., Mol. Opt. Phys. **51**(17), 174004 (2018).
12. S. Witte and K. S. E. Eikema, "Ultrafast optical parametric chirped-pulse amplification," IEEE J. Sel. Top. Quantum Electron. **18**(1), 296–307 (2012).
13. C. Y. Teisset, C. Wandt, M. Schultze, S. Klingebiel, M. Häfner, S. Prinz, S. Stark, C. Grebing, J.-P. Negel, H. Höck, M. Scharun, T. Dietz, D. Bauer, A. Budnicki, C. Stolzenburg, D. Sutter, A. Killi, and T. Metzger, "Multi-kW

Optics EXPRESS

thin-disk amplifiers," in *High-Brightness Sources and Light-driven Interactions*, (Optical Society of America, 2018), p. HT1A.6.
14. T. Nubbemeyer, M. Kaumanns, M. Ueffing, M. Gorjan, A. Alismail, H. Fattahi, J. Brons, O. Pronin, H. G. Barros, Z. Major, T. Metzger, D. Sutter, and F. Krausz, "1 kW, 200 mJ picosecond thin-disk laser system," Opt. Lett. **42**(7), 1381–1384 (2017).
15. C. Y. Teisset, M. Schultze, R. Bessing, M. Häfner, S. Prinz, D. Sutter, and T. Metzger, "300 W picosecond thin-disk regenerative amplifier at 10 kHz repetition rate," in *Advanced Solid-State Lasers Congress Postdeadline*, (Optical Society of America, 2013), p. JTh5A.1.
16. K.-H. Hong, S.-W. Huang, J. Moses, X. Fu, C.-J. Lai, G. Cirmi, A. Sell, E. Granados, P. Keathley, and F. X. Kärtner, "High-energy, phase-stable, ultrabroadband kHz OPCPA at 2.1 μm pumped by a picosecond cryogenic Yb:YAG laser," Opt. Express **19**(16), 15538–15548 (2011).
17. F. Silva, P. K. Bates, A. Esteban-Martin, M. Ebrahim-Zadeh, and J. Biegert, "High-average-power, carrier-envelope phase-stable, few-cycle pulses at 2.1 μm from a collinear BiB3O6 optical parametric amplifier," Opt. Lett. **37**(5), 933–935 (2012).
18. Y. Deng, A. Schwarz, H. Fattahi, M. Ueffing, X. Gu, M. Ossiander, T. Metzger, V. Pervak, H. Ishizuki, T. Taira, T. Kobayashi, G. Marcus, F. Krausz, R. Kienberger, and N. Karpowicz, "Carrier-envelope-phase-stable, 1.2 mJ, 1.5 cycle laser pulses at 2.1 μm," Opt. Lett. **37**(23), 4973–4975 (2012).
19. J. Pupeikis, P.-A. Chevreuil, N. Bigler, L. Gallmann, C. R. Phillips, and U. Keller, "Water window soft-x-ray source enabled by a 25 W few-cycle 2.2 μm OPCPA at 100 kHz," Optica **7**(2), 168–171 (2020).
20. P. Wang, Y. Li, W. Li, H. Su, B. Shao, S. Li, C. Wang, D. Wang, R. Zhao, Y. Peng, Y. Leng, R. Li, and Z. Xu, "2.6 mJ/100 Hz CEP-stable near-single-cycle 4 μm laser based on OPCPA and hollow-core fiber compression," Opt. Lett. **43**(9), 2197–2200 (2018).
21. A. Gordon and F. X. Kärtner, "Scaling of keV HHG photon yield with drive wavelength," Opt. Express **13**(8), 2941–2947 (2005).
22. F. Krausz and M. Ivanov, "Attosecond physics," Rev. Mod. Phys. **81**(1), 163–234 (2009).
23. T. Popmintchev, M.-C. Chen, A. Bahabad, M. Gerrity, P. Sidorenko, O. Cohen, I. P. Christov, M. M. Murnane, and H. C. Kapteyn, "Phase matching of high harmonic generation in the soft and hard x-ray regions of the spectrum," Proc. Natl. Acad. Sci. **106**(26), 10516–10521 (2009).
24. D. Popmintchev, B. R. Galloway, M.-C. Chen, F. Dollar, C. A. Mancuso, A. Hankla, L. Miaja-Avila, G. O'Neil, J. M. Shaw, G. Fan, S. Ališauskas, G. Andriukaitis, T. Balčiunas, O. D. Mücke, A. Pugzlys, A. Baltuška, H. C. Kapteyn, T. Popmintchev, and M. M. Murnane, "Near- and extended-edge x-ray-absorption fine-structure spectroscopy using ultrafast coherent high-order harmonic supercontinua," Phys. Rev. Lett. **120**(9), 093002 (2018).
25. M. Neuhaus, H. Fuest, M. Seeger, J. Schötz, M. Trubetskov, P. Russbueldt, H. Hoffmann, E. Riedle, Z. Major, V. Pervak, M. F. Kling, and P. Wnuk, "10 W CEP-stable few-cycle source at 2 μm with 100 kHz repetition rate," Opt. Express **26**(13), 16074–16085 (2018).
26. L. Young, K. Ueda, M. Gühr, P. H. Bucksbaum, M. Simon, S. Mukamel, N. Rohringer, K. C. Prince, C. Masciovecchio, M. Meyer, A. Rudenko, D. Rolles, C. Bostedt, M. Fuchs, D. A. Reis, R. Santra, H. Kapteyn, M. Murnane, H. Ibrahim, F. Légaré, M. Vrakking, M. Isinger, D. Kroon, M. Gisselbrecht, A. L'Huillier, H. J. Wörner, and S. R. Leone, "Roadmap of ultrafast x-ray atomic and molecular physics," J. Phys. B: At., Mol. Opt. Phys. **51**(3), 032003 (2018).
27. K. Holldack, J. Bahrdt, A. Balzer, U. Bovensiepen, M. Brzhezinskaya, A. Erko, A. Eschenlohr, R. Follath, A. Firsov, W. Frentrup, L. Le Guyader, T. Kachel, P. Kuske, R. Mitzner, R. Müller, N. Pontius, T. Quast, I. Radu, J.-S. Schmidt, C. Schüßler-Langeheine, M. Sperling, C. Stamm, C. Trabant, and A. Föhlisch, "Femtospex: a versatile optical pump–soft x-ray probe facility with 100fs x-ray pulses of variable polarization," J. Synchrotron Radiat. **21**(5), 1090–1104 (2014).
28. Y. Fei, B. Chai, C. Ebbers, Z. Liao, K. Schaffers, and P. Thelin, "Large-aperture YCOB crystal growth for frequency conversion in the high average power laser system," J. Cryst. Growth **290**(1), 301–306 (2006).
29. X. Tu, S. Wang, K. Xiong, Y. Zheng, and E. Sh, "Research on growth and defects of 5 in YCOB single crystal," J. Cryst. Growth **488**, 23–28 (2018).
30. AS-Photonics"SNLO Software," http://www.as-photonics.com/snlo (2019).
31. Tydex, http://www.tydexoptics.com/materials1/materials_for_nonlinear_optics/lithium_niobate/ (2019).
32. R. Maksimenka, G. Jargot, N. Thiré, Y. Pertot, and N. Forget, "Ultra-stable OPCPA at 2 μm, 16 fs, sub 100 mrad CEP noise," in *Mid-Infrared Coherent Sources*, (Optical Society of America, 2020), p. MM3C.3.
33. N. Thiré, R. Maksimenka, B. Kiss, C. Ferchaud, G. Gitzinger, T. Pinoteau, H. Jousselin, S. Jarosch, P. Bizouard, V. D. Pietro, E. Cormier, K. Osvay, and N. Forget, "Highly stable, 15 W, few-cycle, 65 mrad CEP-noise mid-IR OPCPA for statistical physics," Opt. Express **26**(21), 26907–26915 (2018).
34. T. Witting, F. Frank, C. A. Arrell, W. A. Okell, J. P. Marangos, and J. W. G. Tisch, "Characterization of high-intensity sub-4-fs laser pulses using spatially encoded spectral shearing interferometry," Opt. Lett. **36**(9), 1680–1682 (2011).
35. G. Fan, T. Balčiūnas, C. Fourcade-Dutin, S. Haessler, A. A. Voronin, A. M. Zheltikov, F. Gérôme, F. Benabid, A. Baltuška, and T. Witting, "X-SEA-F-SPIDER characterization of over octave spanning pulses in the infrared range," Opt. Express **24**(12), 12713–12729 (2016).
36. T. Balciunas, C. Fourcade-Dutin, G. Fan, T. Witting, A. A. Voronin, A. M. Zheltikov, F. Gerome, G. G. Paulus, A. Baltuska, and F. Benabid, "A strong-field driver in the single-cycle regime based on self-compression in a kagome fibre," Nat. Commun. **6**(1), 6117 (2015).

Optics EXPRESS

37. Andor application note, "Calibrated Soft X-Ray Spectrometer," https://andor.oxinst.com/learning/view/article/calibrated-soft-x-ray-spectrometer (2019).
38. The Center for X-Ray Optics, http://henke.lbl.gov/optical_constants/filter2.html (2019).
39. S. M. Teichmann, F. Silva, S. L. Cousin, M. Hemmer, and J. Biegert, "0.5-keV soft x-ray attosecond continua," Nat. Commun. **7**(1), 11493 (2016).